JITH 2017
18èmes Journées Internationales de Thermique (JITH 2017)
Monastir (Tunisie), 25 - 27 Octobre 2017

The effect of working fluid on the performance of cylindrical heat pipe using Lattice Boltzmann method

Auteurs : Kods GRISSA[1,2], Zied LATAOUI[1], Adel BENSELAMA[2], Yves BERTIN[2], Abdelmajid JEMNI[1]

Adresse des auteurs :
[1] Laboratory of Thermal and Energetic Systems Studies (LESTE) at the National School of Engineering of Monastir, University of Monastir, Tunisia
[2] Institut PPRIME (UPR CNRS 3346), Département Fluides-Thermique-Combustion, ENSMA, 1 av. Clément Ader BP40109, 86961 Futuroscope-Chasseneuil, France

Emails des auteurs : ***kods.grissa@ensma.fr****, zied_lataoui@yahoo.fr, adel.benselama@ensma.fr, yves.bertin@ensma.fr, abdelmajid.jemni@enim.rnu.tn*

Résumé: In the present work, the effect of the working fluid on the performance of cylindrical heat pipe is investigated numerically using Lattice Boltzmann method. Four pure working fluids are tested: water, methanol, ethanol and acetone. Using lattice Boltzmann method, the three regions of heat pipe are modeled including heat transfer in the wall and heat and mass transfer in the liquid-wick and vapor regions. Comparison between the present model and previous numerical results shows very good agreement. The axial and radial liquid velocity profiles and temperature distribution are also presented and discussed. Results indicate superior performance for heat pipe with water as working fluid.

Mots clés :

Heat pipe, working fluid, heat transfer, Lattice Boltzmann method.

1. Introduction

Over the last few decades, the development of devices is still requiring higher heat power and heat power density drainage to overcome their challenging in terms of thermal management constraints. As a reliable and efficient passive cooling device, heat pipes (HP) are promising candidates to meet those constraints with the development of new types of them such as capillary driven heat pipe (CHP) [1], micro heat pipes [2], pulsating heat pipes (PHP) [3] and so on. They provide high heat-power-transfer rates over large distances with minimal temperature drops, excellent flexibility, simple construction, less maintenance and easy control, all with no need for external pumping power [4]. Regarding this usefulness, HPs are currently used in a wide variety of heat transfer related applications such as electronics cooling, renewable energy and space applications [5].

Because of the strong interest in CHP technology and its applications, several theoretical, experimental and numerical analyses have been conducted to help understanding its operation and study its performance at varying space and time levels as reviewed in [5]. The performance of a CHP depends on several elements such the propriety of the working fluid, the nature of the wick structure, etc. Numerous investigations have been carried out on the performance of wicked heat pipe with different working fluid. Experimental studies were performed by Zhang [6] under the condition of pure natural convection, for heating powers from 5 to 60 W, fill ratios from 60% to 90%. Three working fluids were used: FC-72, ethanol, and deionized water. They found that using water as working fluid provides better overall thermal performance once the heating power is greater than a minimum value. However, FC-72 is suggested to be used for low-heat-flux situations, due to its lower minimum heating power. Later, Wong and Lin [7] investigated three different working fluids including water, methanol and acetone, which

possess different figures of merit at the same volumetric liquid charge. Different degrees of wettability were obtained by varying the exposure times in air after the wicked plates were taken out of the sintering furnace. They found the lowered copper surface wettability led to reduced critical heat loads for water rather than for methanol and acetone. From the view of thin-film evaporation mechanism, water has larger surface tension, polarity, viscosity, and latent heat than methanol and acetone. Manimaran et al. [8] conducted experimental investigation on thermal performance of heat pipes using DI-water. Their results indicated that the thermal resistance decreased as the horizontal angle of inclination increased (condenser was elevated) and reached a minimum value when the heat pipe was in vertical position.

In the above-mentioned literature, the Lattice Boltzmann Method (LBM) has never been used to predict the performance of a cylindrical heat pipe with different working fluid, whereas this method was used successfully to deal with similar complicated problems and provided accurate results [9]. Deriving motivation from this fact, the present study aims to describe the heat transfer characteristics of an axisymmetric fluid flow problem in a cylindrical HP using the LBM.

2. Problem definition

The physical configuration of a heat pipe is illustrated in Fig. 1 including the coordinate system used in the present work.

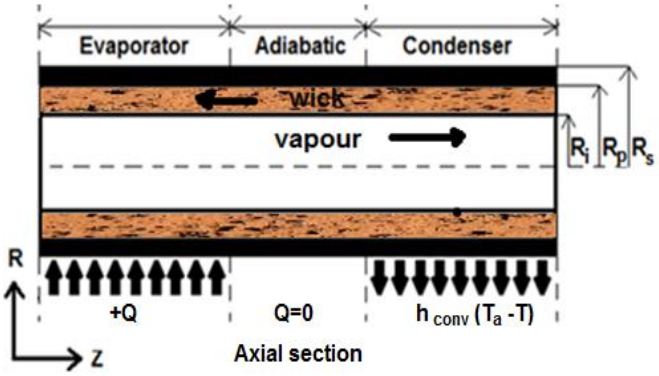

Fig.1. Schematic of conventional cylindrical heat pipe.

The operation of a conventional heat pipe involves the evaporation of a working fluid at the heated end (evaporator section) of the heat pipe. Due to the pressure difference, the resulting vapor moves along the central vapor core length through the adiabatic section toward the cooled end (condenser section) where it condenses by releasing its latent heat of phase change into the provided heat sink. Then, the condensed fluid flows back to the evaporator section end due to the capillary pressure occurring at the menisci in the wick. This process continues long as, for a given heat input in the evaporator section, enough capillary pressure is generated to drive the condensed liquid back to the evaporator. The analysis is carried out for an incompressible, laminar and axisymmetric flow. The porous structure is saturated with a single-phase Newtonian liquid and considered homogenous and isotropic, with uniform porosity and permeability. Furthermore, all the thermophysical properties of the working fluid and solid matrix are assumed constant. Moreover, the viscous dissipation and radiative effects are neglected. When considered, the gravitational acceleration is assumed axial. The liquid and vapor phases are coupled throught the motionless liquid-vapor interface.

3. Governing equations

In this section, the different balances are written for a porous medium filled with liquid. The balances in the vapor region are retrieved from the latter by taking the corresponding thermo-physical properties and letting the porosity approaching unity and the permeability approaching infinity. In the wall region, energy balance is obtained by letting the velocity vanishing, too.

3.1. The governing equations

Under these assumptions, the final form of the local governing equations is given by Eqs. (1) – (4):
Continuity equation:

$$\frac{\partial u_r}{\partial r} + \frac{u_r}{r} + \frac{\partial u_z}{\partial z} = 0 \tag{1}$$

Momentum equations:

$$\frac{\partial u_z}{\partial t} + \frac{1}{\varepsilon}\left(u_r \frac{\partial u_z}{\partial r} + u_z \frac{\partial u_z}{\partial z}\right) = -\frac{\varepsilon}{\rho}\frac{\partial p}{\partial z} + \nu_e \left[\frac{\partial^2 u_z}{\partial r^2} + \frac{1}{r}\frac{\partial u_z}{\partial r} + \frac{\partial^2 u_z}{\partial z^2}\right] + F_{pz} \tag{2}$$

$$\frac{\partial u_r}{\partial t} + \frac{1}{\varepsilon}\left(u_r \frac{\partial u_r}{\partial r} + u_z \frac{\partial u_r}{\partial z}\right) = -\frac{\varepsilon}{\rho}\frac{\partial p}{\partial r} + \nu_e \left[\frac{\partial^2 u_r}{\partial r^2} + \frac{1}{r}\frac{\partial u_r}{\partial r} - \frac{u_r}{r^2} + \frac{\partial^2 u_r}{\partial z^2}\right] + F_{pr}$$

Energy equation:

$$\sigma \frac{\partial T}{\partial t} + u_z \frac{\partial T}{\partial z} + u_r \frac{\partial T}{\partial r} = \alpha_e \left[\frac{\partial^2 T}{\partial z^2} + \frac{1}{r}\frac{\partial T}{\partial r} + \frac{\partial^2 T}{\partial r^2}\right] \tag{4}$$

where u_r, u_z, p and T are the volume averaged radial velocity, axial velocity, pressure and temperature of the fluid, respectively. ν_e is the effective kinetic viscosity is equal to ν the fluid viscosity, the coefficient$\sigma = \left(\varepsilon\rho_f c_{pf} + (1-\varepsilon)\rho_s c_{ps}\right)/(\rho_f c_{pf})$ represents the ratio between the heat capacities of the solid and liquid phases, where ε is the porosity of the porous medium, ρ_f and $\rho_s$are the fluid and solid densities, and c_{pf} and c_{ps} are the fluid and solid specific heats at constant pressure, respectively. α_e is the effective thermal diffusivity coefficient given by:

$$\alpha_e = \begin{cases} \dfrac{\lambda_e}{\varepsilon\rho_l C_{pl}}, & \text{in the porous region} \\ \dfrac{\lambda_v}{\rho_v C_{pv}}, & \text{in the vapor region} \end{cases} \tag{5}$$

where λ_e is the effective thermal conductivity:

$$\lambda_e = \frac{\lambda_l[(\lambda_l + \lambda_s) - (1-\varepsilon)(\lambda_l - \lambda_s)]}{[(\lambda_l + \lambda_s) + (1-\varepsilon)(\lambda_l + \lambda_s)]} \tag{6}$$

From equation (2) and (3), $\boldsymbol{F}_p = (F_{pz}, F_{pr})$ represents the total force including extra viscous terms, due to the presence of porous medium, and body forces, which is given by:

$$\boldsymbol{F}_p = (F_{pz}, F_{pr}) = -\frac{\varepsilon\nu}{K}\boldsymbol{u} - \frac{\varepsilon F_\varepsilon}{\sqrt{K}}|\boldsymbol{u}|\boldsymbol{u} + \varepsilon\boldsymbol{G} \tag{7}$$

where ν is the fluid viscosity; $|u| = \sqrt{u_r^2 + u_z^2}$ and G is the body force induced by an external force, which is given by:

$$\boldsymbol{G} = -\boldsymbol{g}\beta(T - T_0) + \boldsymbol{a} \tag{8}$$

where g is the gravitational acceleration, β is the thermal expansion coefficient, T is the fluid temperature, a is the acceleration due to other external force fields and T_0 is the reference temperature. The geometric function F_ε and the porous medium permeability K are related to the porosit ε based on Ergun's experimental investigations (Ergun 1952), which can be expressed as:

$$F_\varepsilon = \frac{1{,}75}{\sqrt{150}\varepsilon^{3/2}} \tag{9}$$

$$K = \frac{\varepsilon^3 d_p^2}{150(1-\varepsilon)^2} \tag{10}$$

where d_p is the pores' mean diameter.

For the wall region, the heat is transferred purely by conduction as follows:

$$\frac{\partial T_s}{\partial t} = \alpha_s \left[\frac{\partial^2 T_s}{\partial z^2} + \frac{1}{r}\frac{\partial T_s}{\partial r} + \frac{\partial^2 T_s}{\partial r^2}\right] \tag{11}$$

where subscripts "s" refers to solid wall.

The heat transfer problems governed by equations (1)-(4) can be characterized by some dimensionless parameters: the Darcy number Da, the Reynolds number Re, and the Prandtl number Pr, defined as follows:

$$Re = \frac{LU}{\nu}\ , Da = \frac{K}{L^2}, Pr = \frac{\nu}{\alpha_e} \tag{12}$$

where L=Ri and U=Uin are the characteristic length and velocity, respectively.

3.2. Boundary conditions

In order to close the problem, boundary conditions must be provided for each region.
For the wall region:

- $at\ r = r_p\ and\ \ 0 \le z \le L, \lambda_e \frac{\partial T_l(z,r_p)}{\partial r} = \lambda_s \frac{\partial T_s(z,r_p)}{\partial r}$
- $at\ r = r_s\ , \begin{cases} -\lambda_s \frac{\partial T_s(z,r_s)}{\partial r} = -Q, & 0 \le z \le L_e \\ -\lambda_s \frac{\partial T_s(z,r_s)}{\partial r} = 0, & L_e \le z \le L_e + L_a \\ -\lambda_s \frac{\partial T_s(z,r_s)}{\partial r} = h_{conv}(T - T_a)\ , & L_e + L_a \le z \le L \end{cases}$
- $at\ z = 0\ and\ r_p \le r \le r_0,\ \frac{\partial T_s(0,r)}{\partial z} = 0$
- $at\ z = L\ and\ r_p \le r \le r_0\ ,\ \ \frac{\partial T_s(L,r)}{\partial z} = 0$

For the porous region:

- $at\ r = r_i\ and\ \ 0 \le z \le L, u_{z,l}(z,r_i) = 0, u_{r,l}(z,r_i) = u_{r,i}(z,r_i),\ T_l(z,r_i) = T_{sat}(P_i)$
- $at\ r = r_p\ and\ \ 0 \le z \le L,\ u_{z,l}(z,r_p) = u_{r,l}(z,r_p) = 0,\ \lambda_e \frac{\partial T_l(z,r_p)}{\partial r} = \lambda_s \frac{\partial T_s(z,r_p)}{\partial r}$
- $at\ z = 0\ and\ r_i \le r \le r_p, u_{z,l}(0,r) = u_{r,l}(0,r) = 0,\ \frac{\partial T_l(0,r)}{\partial z} = 0$
- $at\ z = L\ and\ r_i \le r \le r_p, u_{z,l}(L,r) = u_{r,l}(L,r) = 0,\ \frac{\partial T_l(L,r)}{\partial z} = 0$

For the vapor region:

- $at\ r = 0\ and\ \ 0 \le z \le L, \frac{\partial u_{z,v}(z,0)}{\partial r} = u_{r,v}(z,0) = \frac{\partial T_v(z,0)}{\partial r} = 0$
- $at\ r = r_i\ and\ \ 0 \le z \le L,\ u_{z,v}(z,r_i) = 0, u_{r,v}(z,r_i) = u_{r,i}(z,r_i), T_v(z,r_i) = T_{sat}(P_i)$
- $at\ z = 0\ and\ 0 \le r \le r_i, u_{z,v}(0,r) = u_{r,v}(0,r) = 0,\ \frac{\partial T_v(0,r)}{\partial z} = 0$
- $at\ z = L\ and\ 0 \le r \le r_i, u_{z,v}(L,r) = u_{r,v}(L,r) = 0,\ \frac{\partial T_v(L,r)}{\partial z} = 0$

At the vapor–porous medium interface the temperature is set to the saturation temperature at the current pressure. Thus, by applying Clausius-Clapeyron equation, the saturation temperature can be determined by:

$$T_{sat} = \left(\frac{1}{T_0} - \frac{R_v}{h_{fg}} ln \frac{P_i}{P_0}\right) \tag{13}$$

where R_v is the gas constant for the vapor, T_0 and P_0 are the temperature and pressure references, respectively. Taking phase change process into account, the energy balance at this interface is given by:

$$Q + \lambda_e \frac{\partial T_l}{\partial r} = \rho_v h_{fg} u_{r,i} \tag{14}$$

IV. Numerical method

As a powerful numerical technique based on kinetic theory analogy, the lattice Boltzmann method (LBM) has proved to be an efficient numerical method for modeling fluid flows in various fields (Li et al. 2016). In this section, the LB model based on the representative elementary volume (REV) approach for axisymmetric thermal flows through porous media is introduced.

IV.1. Formulation of the lattice Boltzmann method for fluid flows though porous media

In this study, the Lattice Boltzmann Method with Double Distribution Function (DDF LBM) approach is used as described in [10]. The model is based on the BGK collision operator and is constructed with the concept of pseudo-Cartesian translation. In this model, the flow field is represented by a Lattice Boltzmann equation (LBE) for the density distribution function, and the temperature field is introduced by another evolution equation of the temperature distribution function. These two functions are presented in the following.

IV.1.1. Velocity field distrubtion function

In order to simulate the axisymmetric flows through porous media, the following LB model was proposed with source and force terms [10]:

$$f_k\left(\boldsymbol{x}+\boldsymbol{c}_k\Delta t, t+\Delta t\right)-f_k\left(\boldsymbol{x},t\right)=\tau_e\left(f_k{}^{eq}(\boldsymbol{x},t)-f_k(\boldsymbol{x},t)\right)+w_k\theta\Delta t+\frac{\Delta t}{6c^2}\boldsymbol{c}_{ki}F_i+F_{pk}\,\Delta t \quad (15)$$

where f_k is the density distribution function (DF) of particles, $f_k{}^{eq}$ is the local equilibrium distribution function (EDF), Δt is the time step, $\mathbf{x}$ is the position vector, *i.e*, $\mathbf{x}$=(z,r), $c=\Delta x/\Delta t$, $\mathbf{c}_{ki}$ is the component of $\mathbf{c}_k$ (the latter being the velocity vector of a particle in the k link), Δx is the lattice size, w_k is the weight, θ is the source term defined by:

$$\theta=-\frac{\rho u_r}{r} \quad (16)$$

F_i is the force term given by:

$$F_i=-\frac{\rho u_i u_r}{\varepsilon r}-\frac{2\rho\nu_e u_i}{r^2}\delta_{ir} \quad (17)$$

and τ_e is an effective relaxation time related to the single relaxation time τ through:

$$\tau_e=\begin{cases}\dfrac{1}{\tau} & ,r=0\\ \dfrac{1}{\tau}\left(1+\dfrac{(2\tau-1)c_{kr}\Delta t}{2r}\right) & ,r\neq 0\end{cases} \quad (18)$$

The last term on the right-hand side of equation (15), $F_{pk}\,\Delta t$, accounts for the total force due to the presence of the porous medium, i.e, Darcy and Forchheimer forces, and other external force fields, i.e, gravity, and is given by:

$$F_{pk}=w_k\rho\left(1-\frac{1}{2\tau}\right)\left[\frac{\boldsymbol{c}_k.\boldsymbol{F}_p}{c_s^2}+\frac{\boldsymbol{u}\boldsymbol{F}_p:(\boldsymbol{c}_k\boldsymbol{c}_k-c_s^2\boldsymbol{I})}{\varepsilon c_s^4}\right] \quad (19)$$

To include the effect of the porous medium, the equilibrium distribution function (EDF) of the DnQb models is defined as follows:

$$f_k^{eq}=w_k\rho\left[1+\frac{\boldsymbol{c}_k.\boldsymbol{u}}{c_s^2}+\frac{\boldsymbol{u}\boldsymbol{u}:(\boldsymbol{c}_k\boldsymbol{c}_k-c_s^2\boldsymbol{I})}{2\varepsilon c_s^4}\right] \quad (20)$$

We used the nine-velocity square lattice (D2Q9) for which w_k is defined by:

$$w_k=\begin{cases}\dfrac{4}{9}, & k=0\\ \dfrac{1}{9}, & k=1,3,5,7,\\ \dfrac{1}{36}, & k=2,4,6,8;\end{cases} \quad (21)$$

and $\mathbf{c}_k$ by:

$$\boldsymbol{c}_k=\begin{cases}(0,0), & k=0,\\ \lambda_k c\left[cos\left(\dfrac{(k-1)\pi}{4}\right),sin\left(\dfrac{(k-1)\pi}{4}\right)\right], & k\neq 0;\end{cases} \quad (22)$$

with λ_k by:

$$\lambda_k=\begin{cases}1, & k=1,3,5,7,\\ \sqrt{2}, & k=2,4,6,8;\end{cases} \quad (23)$$

Accordingly, the fluid density ρ, fluid velocity u and the pressure p are defined by:

$$\rho = \sum_k f_k \tag{24}$$

$$\rho \boldsymbol{u} = \sum_k \boldsymbol{c}_k f_k + \frac{\Delta t}{2} \rho \boldsymbol{F}_p \tag{25}$$

$$p = \frac{c_s^2}{\varepsilon} \sum_k f_k \tag{26}$$

It is noted that the force term $\mathbf{F}_p$ of equation (7) is a function of the velocity **u**. In other words, equation (25) is a nonlinear form of the velocity u. However, due to the quadratic nature of the equation (26), the velocity u can be obtained readily as:

$$\boldsymbol{u} = \frac{\boldsymbol{v}}{c_0 + \sqrt{c_0^2 + c_1 |\boldsymbol{v}|}} \tag{27}$$

where **v** is an auxiliary velocity defined by:

$$\rho \boldsymbol{v} = \sum \boldsymbol{c}_k f_k + \frac{\Delta t}{2} \varepsilon \rho \boldsymbol{G} \tag{28}$$

The parameters c_0 and c_1 in equation (27) are given by:

$$c_0 = \frac{1}{2}\left(1 + \varepsilon \frac{\Delta t}{2} \frac{\nu}{K}\right) \tag{29}$$

$$c_1 = \varepsilon \frac{\Delta t}{2} \frac{F_\varepsilon}{\sqrt{K}} \tag{30}$$

Through the Chapman-Enskog procedure, it can be shown that the effective viscosity is given by:

$$\nu_e = c_s^2 (\tau - 0.5) \Delta t \tag{31}$$

IV.1.1. Lattice Boltzmann for the temperature field

The following LBE is used to describe the evolution of the temperature field, which accounts for the influence of the presence of the solid matrix in the axisymmetric configuration:

$$g_k\,(\boldsymbol{x} + \boldsymbol{c}_k \Delta t, t + \Delta t) - g_k\,(\boldsymbol{x}, t) = \frac{\Delta t}{\tau_g}\left({g_k}^{eq}(\boldsymbol{x}, t) - g_k(\boldsymbol{x}, t)\right) + Q_k \Delta t + w_k\, S \Delta t \tag{32}$$

where g_k is the temperature distribution function (TDF), τ_g is the dimensionless relaxation time which is related to the thermal diffusivity through the Chapman-Enskog expansion:

$$\alpha_e = \sigma {c_s}^2 \left(\tau_g - 0.5\right) \Delta t \tag{33}$$

and ${g_k}^{eq}$ is the equilibrium temperature distribution function that is defined as:

$$g_k^{eq} = w_k T \left[\sigma + \frac{\boldsymbol{c}_k . \boldsymbol{u}}{c_s^2} + \frac{\boldsymbol{u}\boldsymbol{u} : (\boldsymbol{c}_k \boldsymbol{c}_k - c_s^2 \boldsymbol{I})}{2\varepsilon c_s^4}\right] + w_k \frac{\varepsilon P T}{c_s^2 \rho_0} \tag{34}$$

where ρ_0 is the average value of the fluid density.
The source term Q_k is set to:

$$Q_k = w_k \left(1 - \frac{1}{2\tau_g}\right)\left[\frac{\boldsymbol{c}_k . \left(\frac{\varepsilon P \nabla T}{\rho_0} + T \boldsymbol{F}_p\right)}{c_s^2}\right] \tag{35}$$

The last term in equation (32) represents the source term due to the axisymmetric configuration and is given by:

$$S = \frac{\alpha_e}{r} \frac{\partial T}{\partial r} \tag{36}$$

This term can be easily resolved by using Finite Difference method.
Through the TDF, the temperature T of the system is defined by:

$$T = \frac{1}{\sigma} \sum_k g_k \tag{37}$$

IV.2. Boundary conditions

In axisymmetric flows, the distribution functions pointing into the domain have to be defined on all boundaries, including the axis. In the present work, symmetry boundary conditions are applied on the symmetry axis as described by Guo *et al.* [11].

IV. Results and discussions

In this section, the results of the flow and heat transfer in a cylindrical heat pipe are introduced. The effect of the evaporator length, working fluid, wick structure and inclination are discussed. In the numerical calculations, the thermal properties of the working fluids are calculated at the reference temperature and are assumed constant all over the simulation time.

V.1.Code validation

A FORTRAN90 code was developed to solve the governing equations mentioned above by the lattice Boltzmann method.
To check the reliability of the present LBM code, numerical simulations are performed for copper-water wicked heat pipes, wich characteristies are given in Tab. 1.

Tab. 1. The different parameters of the heat pipe [12]

Heat pipe wall	Wick structure	Vapour region
R=0.022 m	r_e=0.02 *m*	r_e=0.0127 *m*
L_{evap}=0.4 m	ε=0.46	ρ_v=0.599 *kg/m*^{3}
L_{ad}=0.2 m	K=0.267×10^{-10} *m*^{2}	λ_v=0.0251 *W/mK*
L_{cond}=0.4 m	ρ_l=960.63 *kg/m*^{3}	μ_v=0.129×10^{-4} *kg/ms*
L_{tot}=1.0 m	λ_l=0.680 *W/mK*	C_{pv}=1888 *J/kg K*
λ_w=387.6 *W/mK*	μ_l=2.8243 *kg/ms*	h_{fg}=225.6267×10^4 *J/Kg*
ρ_w=8978 *kg/m*^{3}	C_{pl}=4216 *J/kg K*	R_v=488 J/kg *K*
T_a=25°*C*	λeff=3.0476 *W/mK*	T_{sat}=373.15 *K*
C_{pw}=381 *J/kg K*	Cpeff=3.8×10^6 *J/kg K*	
h_{conv}=800 *W/m*^{2} *K*	Material: sintered copper	
Material : copper		

The axial and radial dimensionless velocity profiles are plotted in Fig.2 where a heat load of 5000 W/m^2 was applied to the pipe wall along the evaporator. The comparison of the present study with the work of Brahim *et al.* [12] shows an excellent agreement.

(a)

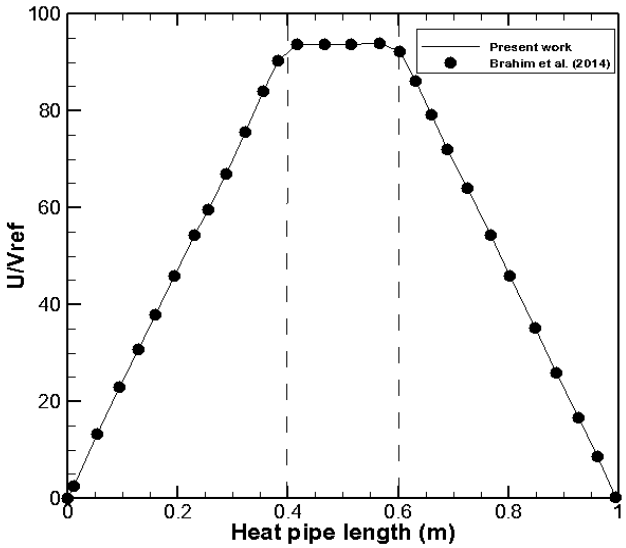

(b)

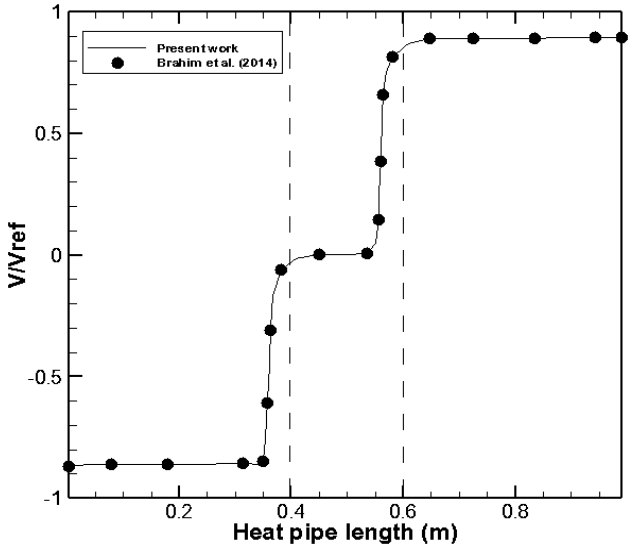

Fig.2.Vapor velocity profile: (a) axial velocity, (b) radial velocity

V.3.Analyze of the thermos-physical properties of the working fluids

In order to study the effect of the working fluid, it is still reasonable to make qualitative analysis and discussions based on its physical propriety. Tab.2 list the most important thermo-physical properties of the four working fluids that affect the HPs heat transfer performance. Previous research showed that the working fluids applied in a HP should have the following characteristics: high value of $(dp/dT)_{sat}$, high latent heat, high specific heat, high surface tension, and low dynamic viscosity. As it can be seen from tab.2, water has the highest thermo-physical properties and the lowest (dP/dT) ratio compared to ethanol, methanol and acetone. Higher dynamic viscosity requires higher force to drive the vapor. Higher boiling point and higher latent heat of vaporisation (LHV) require more energy for the working fluid to actualize phase change and leads to the higher amount of heat. However, a high value of (dP/dT) ratio reveals that a small rise in temperature can generate a large pressure difference and accordingly greater driving force for fluid motion. Under the same flow condition, higher specific heat may result in better sensible heat transfer because the working fluid could bring more energy within each degree centigrade of temperature difference, and higher LHV may lead to better latent heat transfer for more energy could be absorbed or released during phase change (vaporization or condensing) but will hinder the generation and growth of bubbles for the start-up of HP. In heat pipe design, a high value of surface tension is desirable in order to enable the heat pipe to operate against gravity and to generate a high capillary driving force. In addition, it is important factor for the working fluid to wet the wick and container material.

Tab. 2. Thermo-physical properties of the working fluids at standard atmospheric pressure

Working fluids	Boiling point (°C)	Liquid density (kg/m^3)	Thermal conductivity (W/(m°C))	Latent Heat of vaporization (kJ/kg)	Liquid specific heat (kJ/(kg°C))	Dynamic viscosity	$(dp/dT)_{sat}$ $*10^3$(Pa/°C)	Surface tension $*10^3$ (N/m)
Water	100	998	0.599	2257	4.18	1.01	1.92	72.8
Methanol	64.7	791	0.212	1101	2.48	0.60	6.45	22.6
Ethanol	78.3	789	0.172	846	2.39	1.15	4.23	22.8
Acetone	56.2	792	0.170	523	2.35	0.32	6.27	23.7

V.2.Effect of the working fluid

The design of HPs starts with the selection of the working fluid. As it was mentioned in the previous section, the selection of working fluid must be done carefully and it considers several factors. There are a number of candidates for the working fluid that are compatible with copper. For the required operating temperature range of 100°C±20

for solar applications, acetone, methanol, ethanol and distilled water were selected and tested as the possible candidates. However, in addition to being compatible, the fluid must be chemically stable over the operating range of the system and also be non-freezing at very low ambient temperatures. In general, the fluid should be in the liquid phase at the cooler end of the heat pipe and in the vapor phase at the hotter end of the pipe and must be compatible with the outer heat pipe material. Despite the beneficial characteristics of heat pipes, their ability can be restricted by poor thermal properties of the conventional coolant used working fluid. To overcome such problem, the thermal properties of working fluids should be enhanced. Hence, we compared the HP performance by using four different working fluids: acetone, methanol, ethanol and distillated water.

Fig. 3 displays the effect of the working fluid on the temperature distributions. A high value of (dP/dT) ratio reveals that a small change in temperature can generate a large pressure difference, which drives the generated amount of vapor. Therefore, water has delayed the highest steady-state temperature and the liquid pressure compared to other pure fluids. Specific heat of ethanol, acetone and methanol are nearer to each other. But ethanol has 78°C boiling temperature which is higher than acetone and methanol. The ratio of (dP/dT) for ethanol is lower than acetone and menthol. Moreover, ethanol has the highest viscosity among all fluids. High dynamic viscosity increases shear stress along the wall and consequently increases pressure drop in the capillary tube. Therefore, ethanol has delayed the highest temperature and the liquid pressure compared to acetone and methanol. Methanol and acetone have almost same surface tension force. Methanol has little high (dP/dT) ratio compared to acetone but, on the other side, acetone has lower boiling point temperature. Besides, acetone has half viscosity compared to methanol. Lower dynamic viscosity is beneficial due to small shearing force leads to minimum flow resistance.

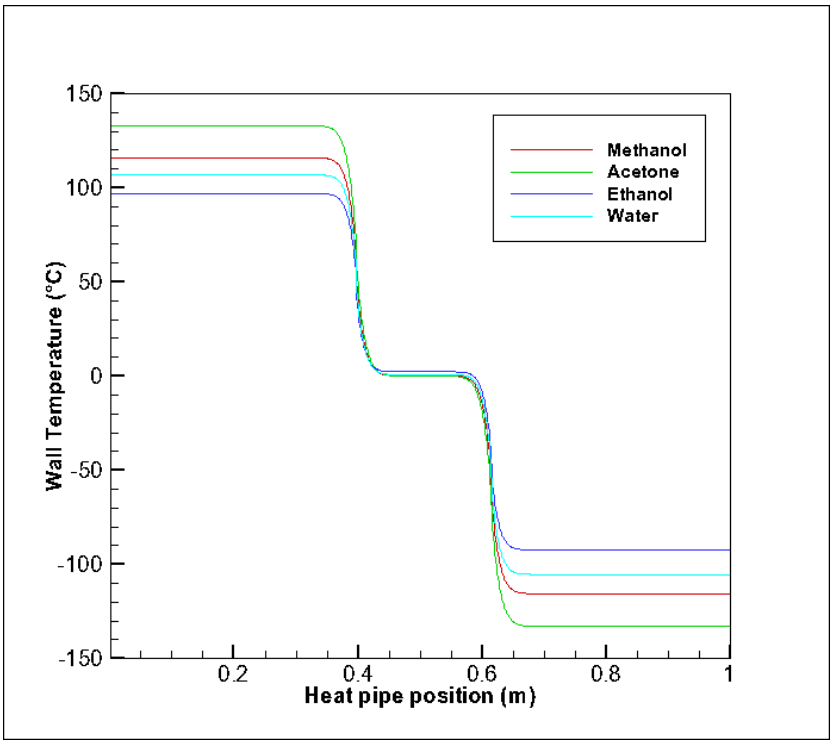

Fig. 3. Liquid pressure and radial wall temperature in in liquid/wick region for different working fluids

The results for the liquid axial and radial velocities are shown in Fig. 4. As it can be seen, the axial velocity along the pipe is divided into three equal parts. The location of the minimum axial velocity quickly migrates into the heat pipe centerline. The velocity distribution gradually approaches a parabolic profile towards the end of the heated region. The velocity distribution is practically symmetric about the heat pipe centerline. This can be explained by the fact that the effective thermal conductivity of the wick is much smaller in comparison to the thermal conductivity of the heat pipe wall. One can see that the liquid in the top wick accelerates in the condenser zone and decelerates in the evaporator zone due to the condensation and evaporation in the corresponding regions. Due to its high density, water moves slowly compared to other working fluids. Whereas, the density value is quite the same for acetone, methanol and ethanol. The observation made is that, the liquid velocity is linear proportional to the density and slower axial liquid velocity results to the reduction in radial velocities in both evaporator and condenser regions.

(a)

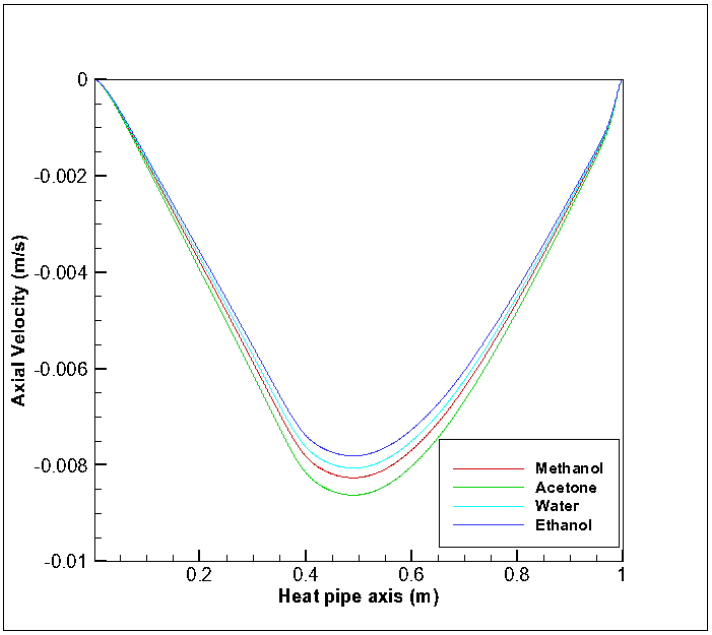

(b)

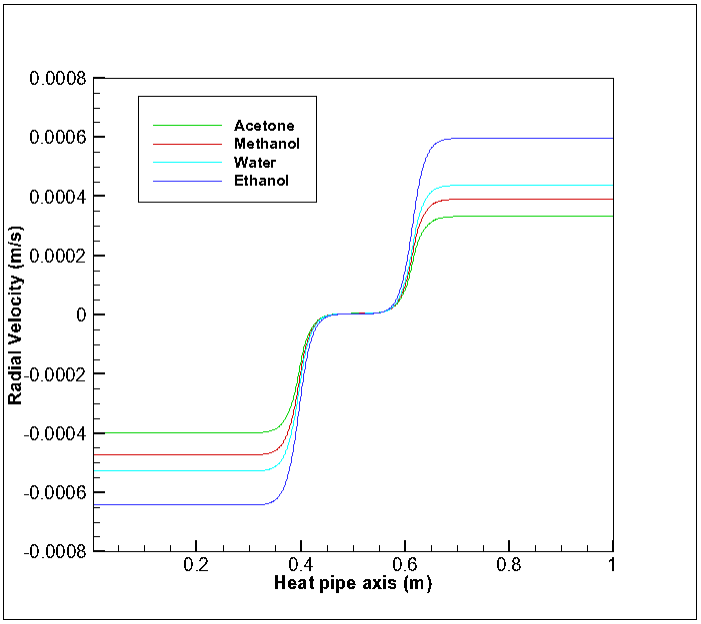

Fig. 4. Liquid axial and radial velocities in liquid/wick region for different working fluids

IV. Conclusion

An investigation of axisymmetric flow inside capillary heat pipes was carried out using Lattice Boltzmann method. Four working fluid were tested. Thermal performance of a HP for various working fluids is also observed to improve with the thermophysical proprieties of the pure fluid. It can be seen that for a constant temperature difference between condenser and evaporator the use of water as the working fluid allows the heat pipe to operate under lowest thermal resistance and then higher performance. Using water based heat pipe is able to perform better than the other working fluids.

Nomenclature

ck	discrete particle velocity
cp	specific heat of the fluid $(J.kg^{-1}.K^{-1})$
cs	lattice speed of sound

Fpk geometric function
Fpr force in the radial direction
Fpz force in the axial direction
Fi external force term for velocity distrubtion function
Fp total body force vector
fk density distribution function in LBE model
f_k^{eq} equilibrium density distribution function
Fε geometric function
G gravitational acceleration
gk temperature distribution function
g_k^{eq} equilibrium temperature distribution function
hfg latent heat of vaporization ($J.Kg^{-1}$)
K permeability of porous media (m^2)
P pressure ($N.m^{-2}$)
Q applied heat flux density ($W.m^{-2}$)
Rp distance between porous insert and pipe's wall

Greek symbols

λ thermal diffusivity ($m^2.s^{-1}$)
β thermal expansion coefficient
ε porosity
θ source term in the energy equation
λ thermal conductivity ($W.m^{-1}.K^{-1}$)
μ dynamic viscosity ($kg.m^{-1}.s^{-1}$)
ν kinetic viscosity ($m^2.s^{-1}$)
ρ fluid density ($kg.m^{-3}$)
σ heat capacity ratio
Δx space step
Δt time step

Subscripts
f fluid
l liquid
s solid
r radial direction
v vapour
z axial direction

References

[1] Hari, R., Jolly, T., & Muraleedharan, C. (2015). Analysis of Two-Phase Flow in the Capillary Wick Structure of Flat Heat Pipe with Different Orientation.
[2] Zhang, J., Diao, Y. H., Zhao, Y. H., Tang, X., Yu, W. J., & Wang, S. (2013). Experimental study on the heat recovery characteristics of a new-type flat micro-heat pipe array heat exchanger using nanofluid. Energy Conversion and Management, 75, 609-616.
[3] Karthikeyan, V. K., Khandekar, S., Pillai, B. C., & Sharma, P. K. (2014). Infrared thermography of a pulsating heat pipe: flow regimes and multiple steady states. Applied thermal engineering, 62(2), 470-480.
[4] Reay, D., McGlen, R., & Kew, P. (2013). Heat pipes: theory, design and applications. Butterworth-Heinemann.
[5] Faghri, A. (2012). Review and advances in heat pipe science and technology. Journal of Heat Transfer, 134(12), 123001.
[6] Zhang, X. M. (2004). Experimental study of a pulsating heat pipe using FC-72, ethanol, and water as working fluids. Experimental Heat Transfer, 17(1), 47-67.
[7] Wong, S. C., Lin, Y. C., & Liou, J. H. (2012). Visualization and evaporator resistance measurement in heat pipes charged with water, methanol or acetone. International Journal of Thermal Sciences, 52, 154-160.
[8] Manimaran, R., Palaniradja, K., Alagumurthi, N., & Velmurugan, K. (2012). An investigation of thermal performance of heat pipe using Di-water. Science and Technology, 2(4), 77-80.
[9] Li, Q., Luo, K. H., Kang, Q. J., He, Y. L., Chen, Q., & Liu, Q. (2016). Lattice Boltzmann methods for

multiphase flow and phase-change heat transfer. Progress in Energy and Combustion Science, 52, 62-105.
[10] Grissa, K., Chaabane, R., Lataoui, Z., Benselama, A., Bertin, Y., & Jemni, A. (2016). Lattice Boltzmann model for incompressible axisymmetric thermal flows through porous media. Physical Review E, 94(4), 043306.
[11] Guo, Z., Zheng, C., & Shi, B. (2002). An extrapolation method for boundary conditions in lattice Boltzmann method. Physics of Fluids, 14(6), 2007-2010.
[12] Brahim, T., & Jemni, A. (2014). Effect of the Heat Pipe Adiabatic Region. Journal of heat transfer, 136(4), 042901.